

ARTICLE OPEN

Various effects of magnetite on international simple glass (ISG) dissolution: implications for the long-term durability of nuclear glasses

Lindsey Neill¹, Stéphane Gin², Thomas Ducasse², Trilce De Echave², Maxime Fournier², Patrick Jollivet², Alkiviadis Gourgiotis³ and Nathalie A. Wall¹

Understanding the effect of near-field materials, such as iron corrosion products, on the alteration of vitreous nuclear waste is essential for modeling long-term stability of these waste forms in a geological repository. This work presents experimental results for which monoliths of International Simple Glass—a six oxide borosilicate glass—, with polished and unpolished cut sides, were aged for 70 days under oxic conditions at 90 °C in a solution initially saturated in $^{29}\text{SiO}_2$ at pH 7; then magnetite was added to the leaching environment. Solution and solid analyses were performed to correlate the changes in the surface features and dissolution kinetics. It was found that magnetite primarily influences the mechanically constrained surface of the non-polished sides of the monoliths, with little to no effect on the polished surfaces. This work highlights the importance of the unique chemistry within surface cracks that invokes a drastic change in alteration of glass in environments containing iron corrosion products.

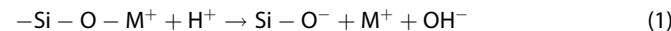
npj Materials Degradation (2017)1:1 ; doi:10.1038/s41529-017-0001-6

INTRODUCTION

Confinement within a borosilicate glass matrix is currently proposed for the disposal of radionuclides remaining from used nuclear fuel from power reactors.¹ In France, glass containing ~18% (w/w) waste is poured into a stainless steel canister. Before disposal in a deep geological repository, the canister will be placed into a several centimeter thick carbon steel over pack.² A better understanding of the interactions between glass and iron and the associated iron corrosion products is necessary to assess the performance of these waste forms.³

Work has been performed to understand the fundamental mechanisms controlling glass dissolution under a variety of conditions and link these mechanisms to the overall kinetics of glass behavior.⁴ The processes that control glass dissolution in a geological repository involve a complex set of reactions, which depend on the nature of the host rock, the near field materials, the temperature, the ground water composition along with its renewal rate, and the glass composition.^{5–13} The ultimate goal for laboratory scale parametric studies of glass alteration is to build an accurate predictive model that can account for the kinetics of long-term glass alteration under a variety of relevant conditions.^{14–16} Experimental validation of these predictive models under accelerated conditions at a laboratory time scale is not possible as glass dissolution is controlled by coupled non-linear processes, therefore validation instead relies on the study of archeological and basaltic glasses altered in well understood geochemical conditions.^{17–20} A more thorough understanding of all mechanisms and the associated kinetics of not only the glass itself but with the surrounding environment must be achieved to build a robust model.

Literature pertaining to borosilicate glass dissolution demonstrates that silica species play a major role in the mechanisms and associated kinetics. In dilute conditions, water begins to diffuse into the glass matrix (hydration) and alkali ions exchange with the positively charged hydrogen species (interdiffusion) (Eq. 1).^{21–25} Hydrolysis of the silicon network also begins with silica being released into solution (Eqs 2 and 3).^{26, 27} The corresponding kinetic regime is designated as the *initial* or *forward rate*, r_0 .



As the dissolved silica concentration increases, the rate decreases to a *residual rate*, r_r . The rate decrease is attributed to a decrease of the affinity of the hydrolysis of the silicate network and the formation of an amorphous layer (i.e., gel) that becomes transport-limiting in silica saturated conditions.²⁸ Two different mechanisms are proposed for the formation of this gel layer. One mechanism is based on the precipitation of a silica rich layer on the glass surface; the second mechanism is based on in-situ re-condensation of the silicon oxygen bonds, forming a porous gel layer on the glass surface. Previous studies have made use of isotopic tracers to differentiate between these two mechanisms, allowing a greater understanding of the exchange of silicon between the bulk solution and glass surface.^{29–32} These studies demonstrated that a combination of both mechanisms may occur, which is dependent on the solution pH and the reaction progress.

There is also a possibility of an alteration resumption, commonly attributed to the rapid precipitation of secondary

¹Chemistry Department, Washington State University, Pullman, WA 99163, USA; ²CEA Marcoule, DE2D SEVT, F-30207 Bagnols-sur-Cèze, France and ³Institut de Radioprotection et de Sûreté Nucléaire, PRP-DGE/SRTG/LT2S, Fontenay-aux-Roses, France

Correspondence: Stéphane Gin (stephane.gin@cea.fr) or Nathalie A. Wall (nawall@wsu.edu)

Received: 24 October 2016 Revised: 9 December 2016 Accepted: 27 December 2016

Published online: 25 July 2017

phases.³³ Under this regime, zeolites, and calcium silicate hydrates form at the expense of the passivating film. Additionally, environmental components, such as organic molecules or iron corrosion products, can have detrimental effects on the passivating layer.^{34, 35} Glass compositions, such as those high in aluminum, and solution pH are two key factors controlling this regime.³⁶

Iron and its associated corrosion products (primarily siderite and magnetite) have been seen to enhance glass alteration via the sorption of silica onto the surface of the iron-rich phases and the precipitation of iron silicate minerals.^{37–43} Each of these processes shifts the equilibrium established between the glass surface layers and surrounding solution; glass alteration rates are directly dependent on the availability of iron.

In addition to sorption of silica on the iron surface and precipitation of iron silicates, magnetite influences SON68 glass behavior, the French high level waste reference glass. A study describing the effect of magnetite on SON68 proposes two other processes: 1) precipitation of SiO_2 on the magnetite surface and 2) iron incorporation into the glass alteration layers with potential modifications of the transport properties of the gel itself.³⁵ The present study provides evidences that these processes occur, although iron incorporation into the alteration layer is not seen until months after the addition of magnetite. Thus, this process would be highly dependent on iron availability in solution that is resulting from magnetite dissolution. This demonstrates that the iron–glass relationship is complex and that additional information is still needed to explain mechanisms and kinetics of glass behavior.

The formation of cracks at the glass surface also contributes to the overall durability of the glass matrix, primarily because surface cracks increase the reactive surface area. While molten glass cools within the carbon steel over pack, the temperature gradient between the perimeter and core of the glass leads to thermic shock-induced cracks. These cracks (also called defaults) provide preferential sites for alteration on a small scale, such as diffusion of alkali ions into the surrounding environment.⁴⁴

Experimentally, defaults within the glass matrix are also observed during cooling and sample preparation (e.g., cutting).^{45, 46} These processes are mechanically violent and generate a high number of micro cracks, or Griffith cracks, due to the metastable nature of the glass structure.⁴⁷ Griffith summarized that the strength of the material was dependent on defects such as these surface cracks. These Griffith cracks can spontaneously propagate due to external factors such as mechanical stress or chemical gradients. The evolution of these micro cracks into larger cracks can be compared to dislocations in crystals due to grain boundaries. Though the defaults are caused by different methods (formation vs. processing), the investigation of the alteration of non-polished glass surfaces can give insight into the alteration of the cracks seen in large-scale waste materials.

The goal of this study is to further understand the alteration of the glass waste form in the presence of iron corrosion products, specifically magnetite (iron (II,III) oxide). This study is an extension of a similar experiment recently performed, in which experimental conditions are similar to that of the present work, except that the present work includes the addition of an iron source.³⁰ Comparison of results of this work with a reference experiment without an iron source allows for a better understanding of the alteration layer properties. The experiment was carried out in conditions initially saturated in ^{29}Si to follow the isotopic exchange of silicon between the solution and glass to monitor changes of the alteration layer. Additionally, five of the six sides of the glass monoliths were unpolished which provides insights into the effect of surface cracks on the alteration progress of the glass.

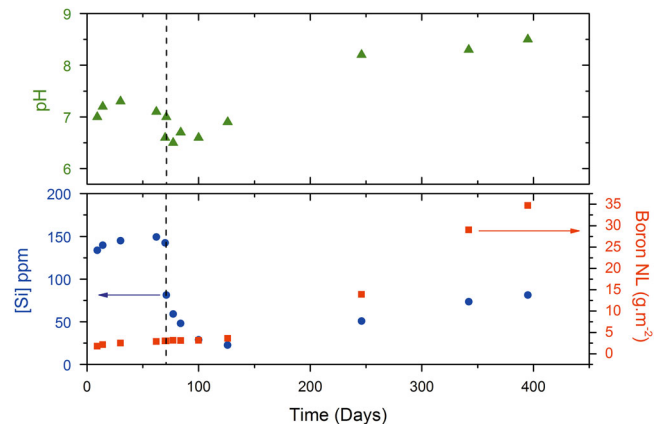


Fig. 1 Upper graph shows the pH (green triangles) during the experiment. For each time point, the pH was measured and then adjusted back to 7, except for the last three time points. Lower graph shows the change in Si concentration (blue circles, bottom left axis) and the NL (red squares, bottom right axis) calculated from the boron concentration in solution. Resumption of alteration is seen at day 246 based on the increased concentration of boron and silicon in solution

RESULTS

Solution analysis

Results from inductively coupled plasma–optical emission spectroscopy (ICP-OES) for individual glass constituents and multi-channel inductively coupled plasma–mass spectrometry (MC-ICP-MS) for silicon isotope concentrations are shown in Table 1.

Figure 1 presents the silicon concentration, normalized loss (NL) based on boron solution conditions, and pH over the experiment time period. The pH was maintained during the 150 first days by monitoring the solution and correcting to pH 7 using 0.5 M HNO_3 or 0.5 M KOH. The pH was measured but not adjusted after the first 150 days; the pH then slowly increased to eight. This allowed the pH to drift to a pH at which orthosilicic acid starts dissociating into anions (H_3SiO_4^- , $\text{H}_2\text{SiO}_4^{2-}$...), this seems to have an insignificant effect on the glass dissolution rate (Fig. 2), which remains essentially constant between day 126 and day 395. Over the first 2 months, the glass was allowed to react in a solution saturated with amorphous silica under the same experimental conditions as seen in Gin et al.³⁰ In the present work, magnetite was added 70 days after the experiment was initiated and a significant decrease in the concentration of silicon was observed almost immediately, with a decrease of ~60 p.p.m. of silicon within the first day after magnetite addition. This decrease extends for 2 months after the addition of magnetite, at which point the solution only contains 22 p.p.m. of silicon. The last data points (up to nine months after the addition of magnetite) show the resumption of alteration.

Figure 2 presents the alteration rate changes over the duration of the experiment based on the boron concentrations in solution. The rate continues to decrease after the addition of magnetite at day 70, although the rate never reaches the long term rates of 0.1 nm per-day observed by Gin et al.³⁰ After ~100 days, the alteration rate increases. The rate reaches a maximum of ~100 nm per-day for the rest of the experiment duration. While this is a large increase, the long-term rate never reaches the value observed at day one of this experiment (500 nm per day).

Figure 3 demonstrates three different regimes involving the isotopic silicon concentrations. The system is in equilibrium before the addition of magnetite, where surface layers form with little or no exchange of Si species in solution, as previously demonstrated.³⁰ The second regime lasts between days 70–126, during

Table 1. ICP-OES and MC-ICP-MS analysis of solution sampled at various time points

Time Days	pH _{90°C}	AGF %	Si mg L ⁻¹	ICP-OES					MC-ICP-MS			
				B mg L ⁻¹	Ca mg L ⁻¹	Na mg L ⁻¹	Fe mg L ⁻¹	K g L ⁻¹	²⁸ Si mg L ⁻¹	²⁹ Si mg L ⁻¹	³⁰ Si mg L ⁻¹	TOTSi mg L ⁻¹
0.4	7.2	0	140.0	<0.1	0.9	6.3	BD	3.5	2.1	135.4	2.4	140.0
9	7.0	0.18	133.8	6.7	5.7	16.7	BD	3.7	—	—	—	—
14	7.2	0.21	139.7	8.1	7.3	20.2	BD	3.8	15.4	122.8	1.5	139.7
30	7.1	0.25	144.9	9.5	6.8	20.8	BD	3.7	16.7	126.7	1.6	144.9
62	7.1	0.29	149.2	10.9	9.2	23.5	BD	3.8	18.0	129.5	1.7	149.2
70	6.6	0.30	142.5	11.6	8.4	25.0	BD	3.0	8.0	133.3	1.3	142.6
71	7.0	0.30	81.2	11.8	12.9	29.7	BD	3.0	7.9	73.1	0.9	81.3
77	6.5	0.32	59.4	12.6	14.7	32.4	BD	2.9	6.7	51.6	0.8	59.1
84	6.7	0.32	48.1	12.6	11.9	32.8	BD	3.0	9.5	37.7	0.8	48.1
100	6.6	0.32	28.7	12.9	10.6	33.8	BD	3.1	7.7	20.4	0.6	28.7
126	6.9	0.37	22.6	15.2	9.8	37.6	BD	3.5	2.3	18.4	0.2	21.0
246	8.2	1.61	50.7	65.3	13.7	121.9	0.06	4.2	27.3	11.8	1.84	40.9
342	8.3	3.37	73.6	126.2	28.2	227.4	BD	3.7	—	—	—	—
395	8.5	4.68	81.3	149.6	29.0	278.8	BD	3.6	—	—	—	—

BD indicates that the value for that element was below the 0.1 mg L^{-1} detection limit. Dotted line represents the addition of magnetite 'AGF' stands for altered glass fraction and '—' within the MC-ICP-MS data denotes that the sample was not analyzed at that time point. There is a 10% uncertainty on each element measured by ICP-OES except Na which has a 50% error due to contamination within the K salts used to synthesize the potassium silicates during alkaline fusion. These potassium silicates were used to prepare the initial solution of 150 p.p.m. Si. Elements measured by MC-ICP-MS have a 5% error due to matrix effects. The dotted horizontal line represents the addition of magnetite.

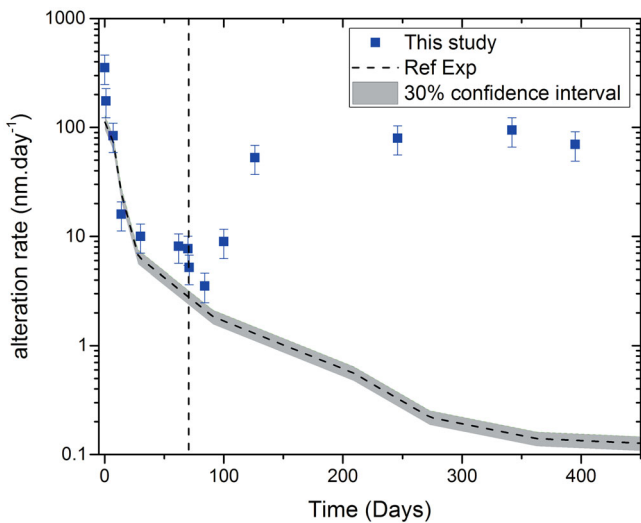


Fig. 2 Rates of alteration calculated based on a linear regression of the equivalent thickness determined at each time point. The gray dotted line represents the rates observed for the reference experiment with a 30% confidence interval (gray shading).³⁰ The black dotted line represents the addition of magnetite at day 70

which the available Si in solution is consumed, either by sorption or precipitation on the magnetite surface or iron silicate precipitation. The third regime continues beyond 126 days; Si concentration increases, though only ^{28}Si and ^{30}Si increase while ^{29}Si continues to decrease. This demonstrates that later time points are a resumption of alteration of the glass itself. If the increased concentrations of Si were due to dissolution of the silicon sorbed on the magnetite surface, ^{29}Si concentrations would have risen as well.

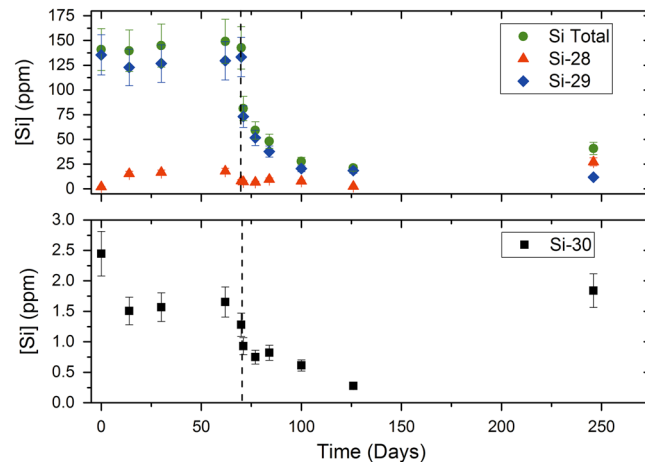


Fig. 3 ^{28}Si , ^{29}Si , ^{30}Si concentrations, as determined by MC-ICP-MS solution analyses. The lower graph shows only ^{30}Si as it makes up less than 1% of the total Si concentration. The dotted black line represents the addition of magnetite at day 70

Time-of-Flight Secondary Ion Mass Spectrometry (TOF-SIMS) analysis of the glass monoliths

In addition to monitoring changes by solution analysis, changes of mobile elements within the alteration layer were analyzed using TOF-SIMS. Monoliths were withdrawn from the solution at day 70 (immediately before the addition of magnetite), day 84 (2 weeks after addition), day 126 (2 months after addition) and day 246 (almost 6 months after addition). Figure 4 shows the analysis of the polished face of the monolith at day 70, with the three mobile species (B, Na, and Ca) showing inverse correlation with the hydrous species (H). Sodium and calcium are known to exhibit this sigmoidal profile due to preferential dissolution of these elements,

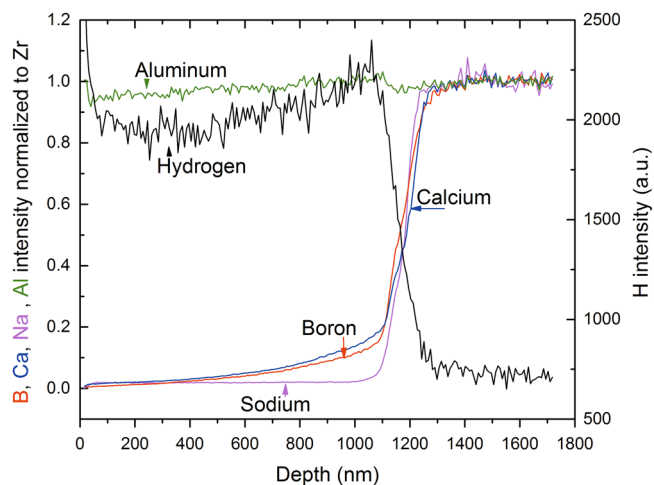


Fig. 4 TOF-SIMS derived elemental profiles of the major glass constituents of a monolith withdrawn at day 70, immediately before the addition of magnetite. This allows for a direct comparison of the monoliths with the reference experiment before the system was disturbed.³⁰ All elements, except H, are normalized to Zr, as this element is immobile during alteration and to their concentration in the pristine glass, which allows for a qualitative comparison between the elements

with similar behavior by boron.³⁰ While boron may not be released by the same mechanisms as the alkali species, the low energy barrier to break the B–O–Si bonds allows for a similar profile.⁴⁸

The potential inclusion of iron into the alteration layers formed on the polished face of the monoliths was also studied by TOF-SIMS (Fig. 5). Significant iron incorporation into the alteration layer is not seen until day 246. Data for monoliths from day 83 and 126 demonstrate an increase of iron within the first nanometers of the sample, but this could be contributed to magnetite grains adhering to the surface instead of being incorporated into the alteration layer. While iron-containing secondary phases are commonly observed in the literature studies mentioned in the introduction, these results suggest that iron incorporation takes place after the reactions that occur at the magnetite surface. This could also be due to the time it takes for the dissolution of magnetite to introduce iron into the solution since the magnetite and glass surfaces were not in contact. These profiles also show that there is not a significant increase in alteration layer thickness, based on the boron profile, even after the addition of magnetite and calculated resumption of alteration. Since only the polished side of the monolith was analyzed by TOF-SIMS, this suggests that the behavior of the polished and unpolished sides strongly differ.

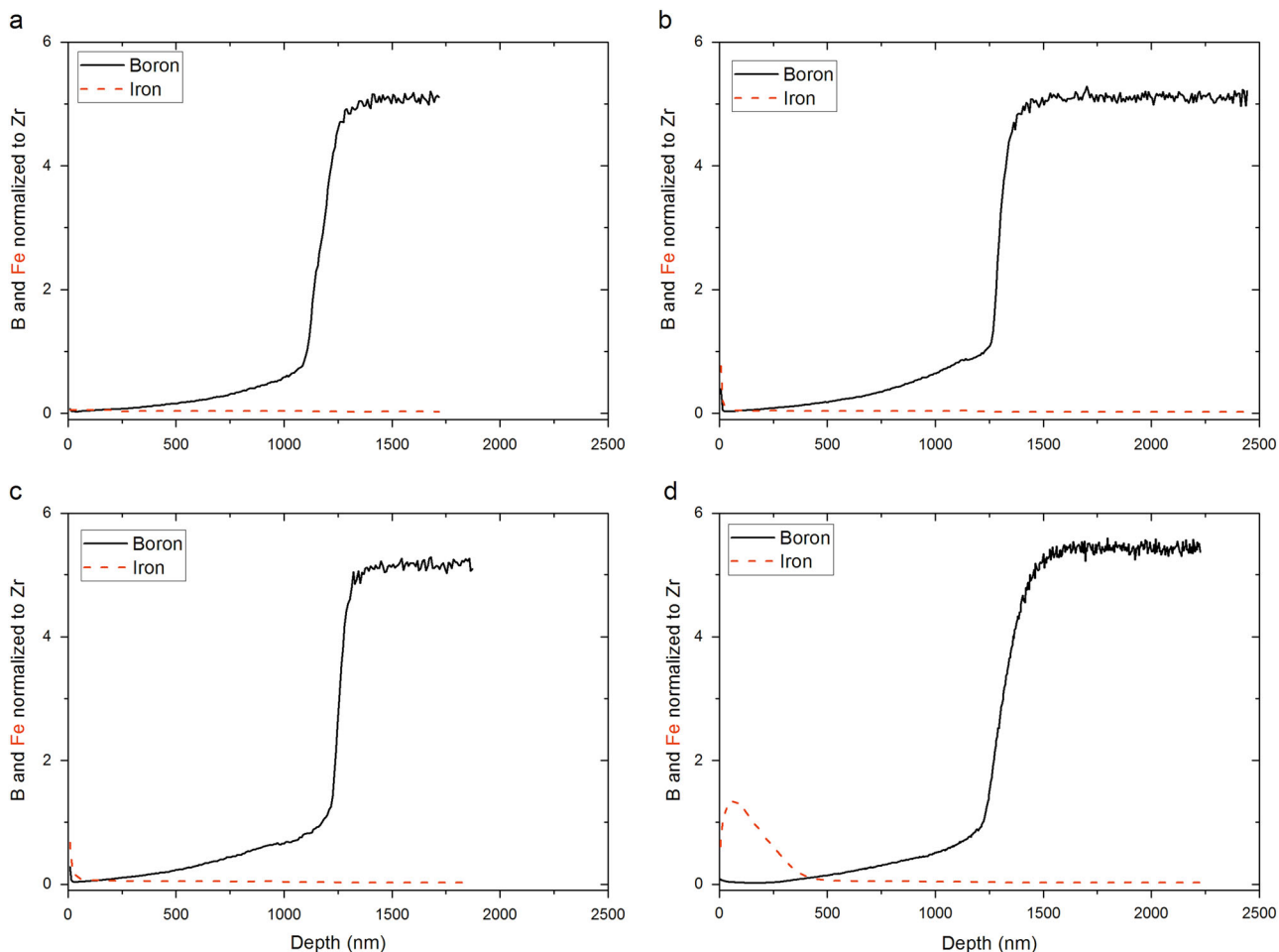


Fig. 5 TOF-SIMS elements profiles for iron (red) and boron (black) of the polished surface of each monolith. The boron profile is shown as a measurement of the alteration layer thickness at each time point. **a** day 70: before addition of magnetite $E_{th} = 1.17 \mu\text{m}$; **b** day 83: 2 weeks after addition $E_{th} = 1.29 \mu\text{m}$; **c** day 126: 2 months after addition $E_{th} = 1.25 \mu\text{m}$; **d** day 246: 6 months after addition $E_{th} = 1.26 \mu\text{m}$. Depths were measured by profilometry during TOF-SIMS analysis

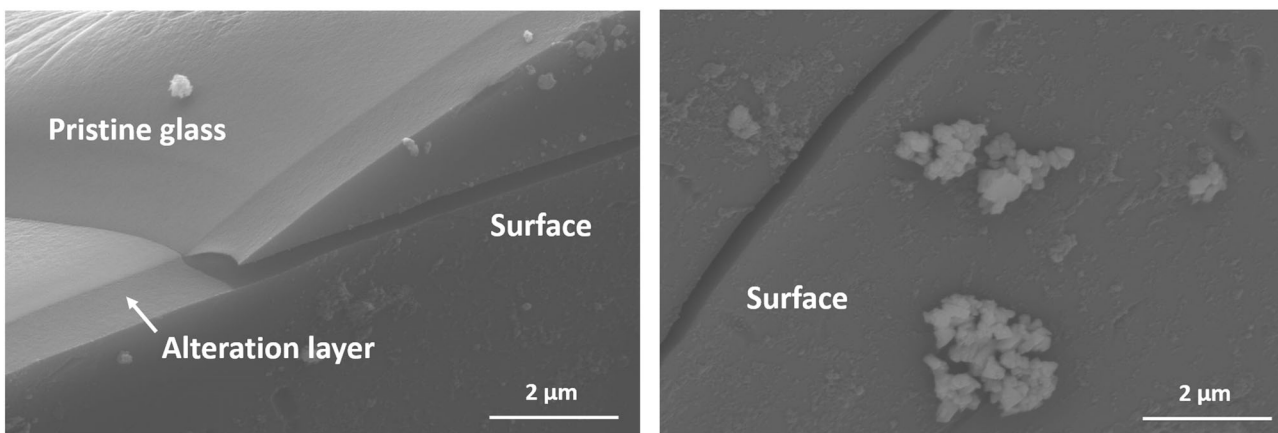


Fig. 6 SEM image of polished surface of day 126 monolith. Secondary phases, not observed for earlier samples, have now begun to form. *Left image* shows all three portions of the glass (pristine, alteration layer, and surface). The image on the *right* shows a close up of the secondary phases seen on the surface

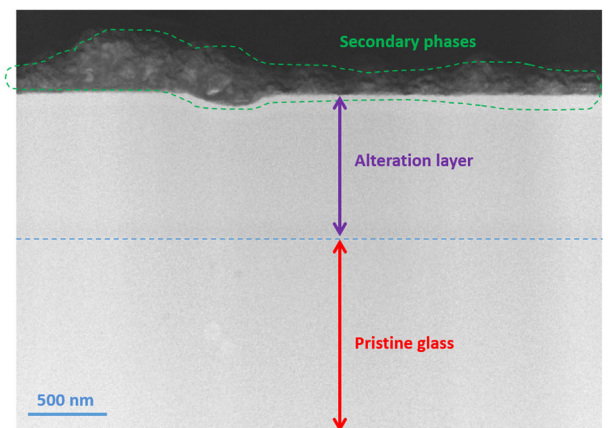
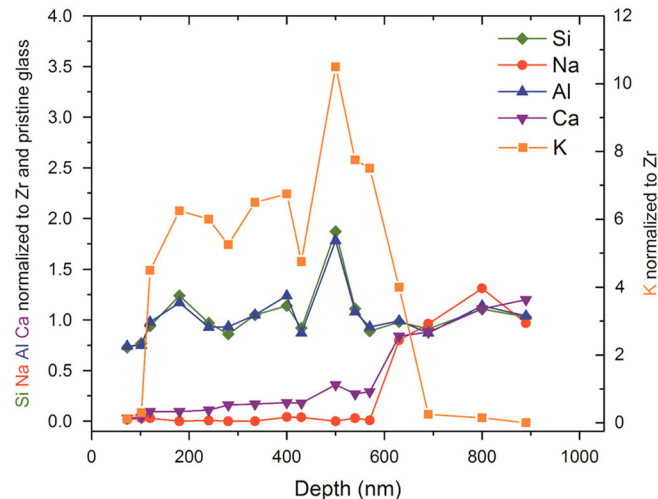


Fig. 7 TEM image on the left of polished side of day 246 monolith. Alteration layer of $\sim 1 \mu\text{m}$ is seen with an additional 300 nm of secondary phases on the surface. The absence of contrast inside the alteration layer shows that there is no porosity formed within the alteration layer or that the pore size is smaller than 5–10 nm. The *right* figure shows the EDS profile of this alteration region. Iron was not detected within the gel by this method

Transmission Electron Microscopy (TEM)/Scanning Electron Microscopy (SEM) of glass and magnetite surfaces

Polished faces of the monoliths withdrawn at days 70, 84, and 126 were analyzed by SEM to monitor the growth of secondary phases and any surface features. The polished side of the monolith withdrawn at day 246 was analyzed by TEM. Figure 6 shows images of a tilted sample for day 126. No secondary phases were observed until this time point. Energy dispersive spectroscopy (EDS) shows that no iron-containing secondary phases formed on this side of the monolith. A cross section of the same monolith was analyzed by SEM to calculate an alteration layer thickness of 1.26 μm .

Figure 7 shows the TEM image of a monolith withdrawn at day 246. This demonstrates an alteration layer thickness of 1 μm with a 300 nm secondary phases. Electron diffraction analysis showed that no crystalline phases were present and that significant amount of iron was incorporated in the alteration layer. EDS analysis could not identify the secondary phases due to the presence of large quantities of the deposited metals such as gold and platinum. However, based on their morphology, iron silicate minerals are highly suspected.



SEM analysis of a monolith withdrawn from the experiment at day 358 showed that significant changes at the glass surface had occurred. Figure 8 shows the alteration layers on the non-polished surfaces of the monolith that now contain sections of alteration associated with cracks in the glass surface. These cracks prove to be a critical feature in the alteration of the glass surface. The majority of the alteration takes place primarily at these points instead of a uniform alteration across all surfaces, as there does not seem to be a change in alteration thickness on the polished surface. EDS mapping shows an additional layer containing iron on the glass surface.

TEM and SEM observations were also performed on a sample of magnetite withdrawn at day 246; results are presented with Fig. 9. TEM EDS analysis shows clusters with increased concentrations of silicon outside the grain boundary confirming the precipitation of silica or iron silicate on the surface of the magnetite. Silicon peaks are seen along with potassium and calcium which indicate that silicates are precipitating on the surface of the magnetite in addition to silicon sorption. SEM images show the entire surface of the magnetite grains is covered with a silicon rich secondary phase.

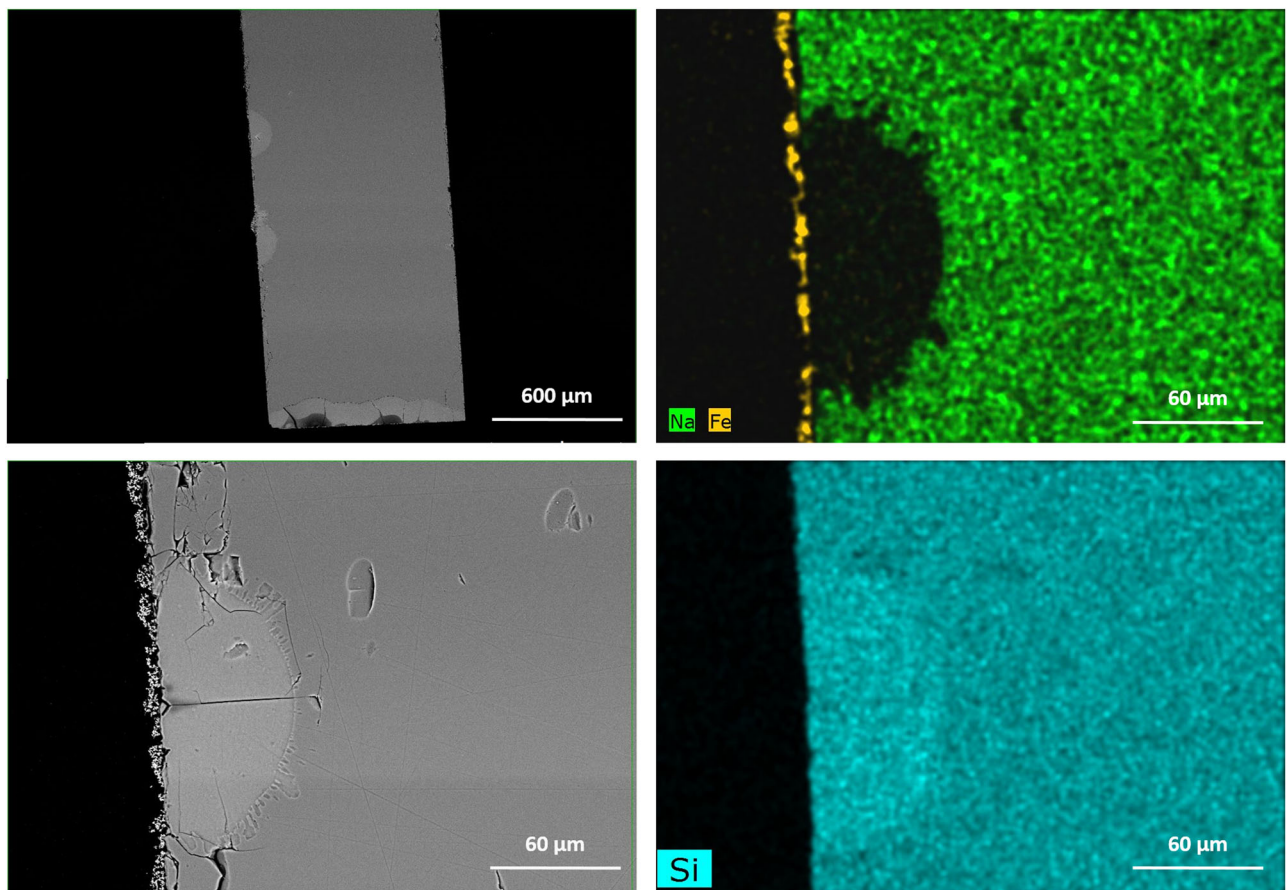


Fig. 8 SEM images of day 358 non-polished surface of the monolith. In the upper left, the total monolith is shown with the polished side on the right. Areas of enhanced alteration are seen on all unpolished surfaces. Bottom left image shows a magnification of one of the altered areas that surrounds a crack in the surface. The images on the right show EDS mapping of significant elements denoting the alteration area and a concentrated area of iron on the surface

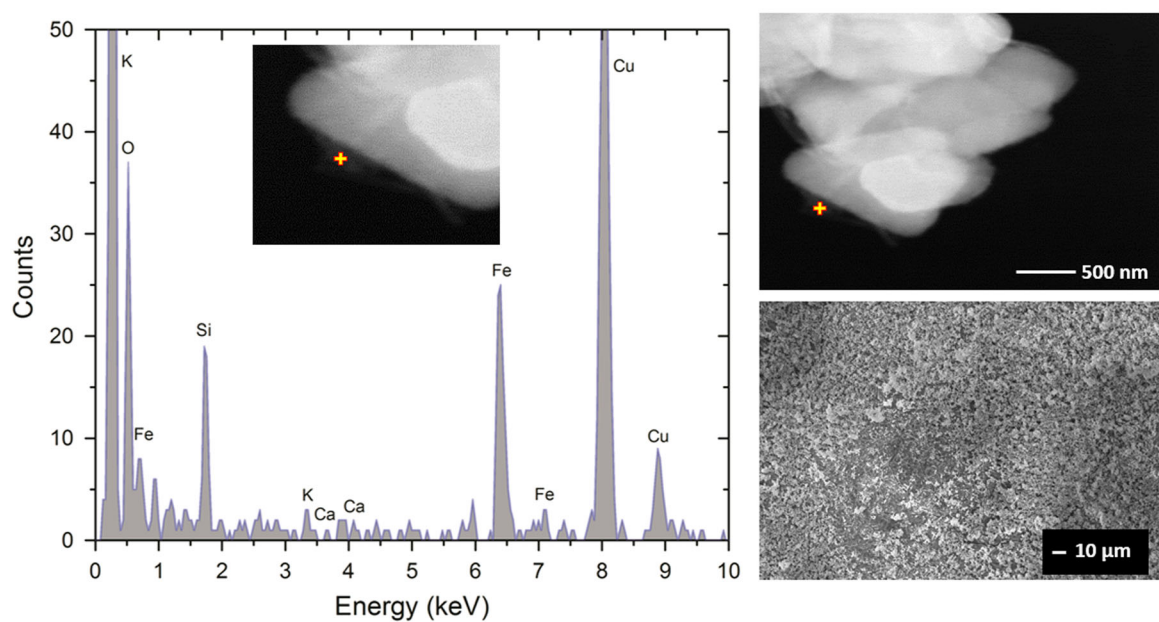


Fig. 9 TEM image and EDS analysis of a magnetite grain. Upper right image shows the TEM analysis of the grain with the corresponding EDS spectra on the left image. SEM of the magnetite grains is shown on the bottom right

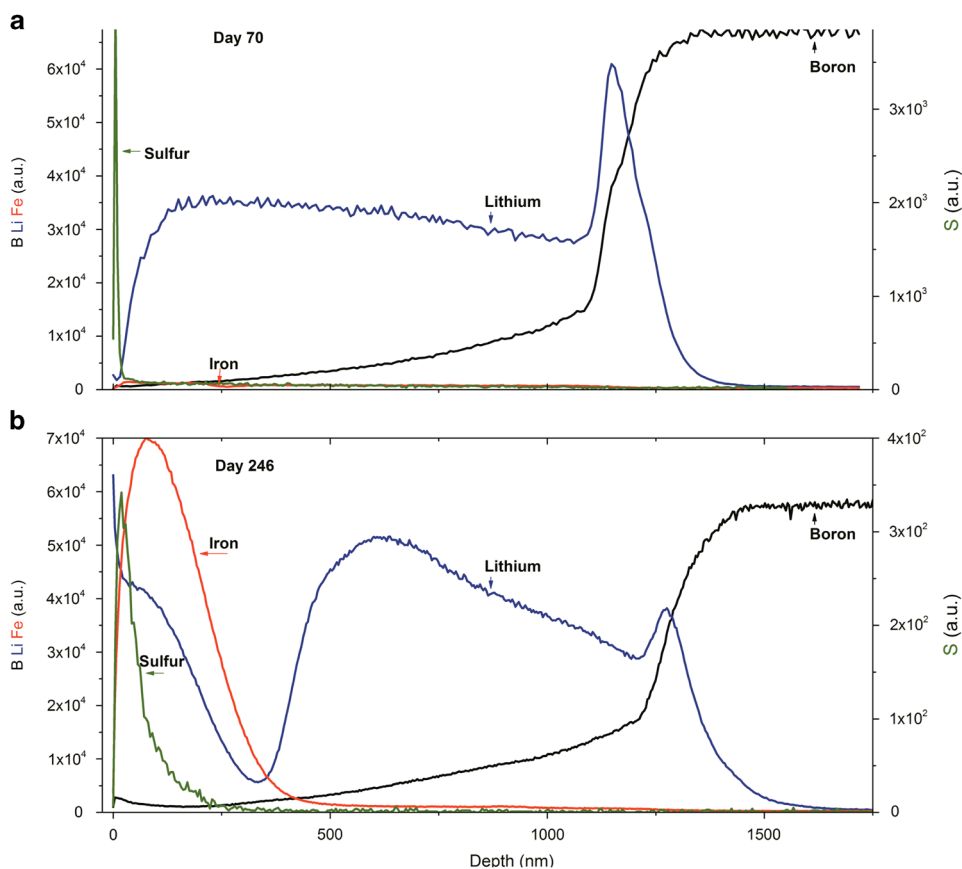


Fig. 10 TOF-SIMS elemental profiles of polished surface of monoliths sampled at (a) day 70 and (b) day 246, after tracing experiment with lithium and methylene blue (denoted by sulfur). Significant changes are seen in the first 250 nm of the day 246 sample

Behavior of diffusive species

Monoliths withdrawn at day 70, 84, 126, and 246 were subjected to a post tracing experiment to further understand the diffusivity changes within the alteration layers of the polished faces. The behavior of iron into the surface as well as methylene blue, a non-reactive 1 nm diameter molecule, and Li, which has been shown to diffuse into the pristine glass at a rate higher than other hydrous species, were monitored.⁴⁹ Figure 10 shows a comparison of a monolith before the addition of magnetite and 6 months after addition (at which time iron was seen incorporated into the alteration layer). Since these components are not within the glass composition they cannot be normalized and thus only give a qualitative view of diffusion into the alteration layers.

At day 70, just before the addition of magnetite, only lithium diffusion is seen, suggesting the pores diameters are too small to allow ingress of large molecules. Methylene blue is seen only within the first few nanometers, implying that only molecules of the dye are adhering outside of the monolith instead of diffusing into the alteration layers. These results are consistent with those published in the literature, which confirms that a dense layer made of sub-nanoporous amorphous silica acts as a molecular sieve for aqueous species.^{30, 31} At day 246, two distinct layers are observed, one with increased iron concentrations and the common alteration layer seen at all time points. Lithium partitions between these two layers, with a decrease at the alteration layer pristine glass interface, while it is still incorporated into the gel layer and into the pristine glass. Methylene blue is also present in the secondary iron-containing layer up to the interface of these two alteration layers. In the reference experiment, methylene blue also diffused 250 nm into a monolith sampled at day 209.³⁰ Since

this 250 nm cutoff was observed in both the reference experiment and the present work featuring iron, it suggests that iron is not responsible for this secondary layer, but that this outer 250 nm layer contain pores with diameters large enough to incorporate larger ions.

Although there is a significant interface between an iron-bearing layer and the common alteration layer, this is most likely due to the nature of the alteration layer and pore diameters of this region instead of an iron affecting the properties or porosity of the alteration layer itself. It must be noted that although iron is seen within the alteration layers, the quantity of iron is not known as this method is only qualitative. Therefore, while the exact concentration of iron is not known, iron is most likely present at a low concentration based on the lack of iron detected by EDS as shown in Fig. 7.

DISCUSSION

Differences in alteration layer thicknesses

Analyses of the alteration layers by multiple methods demonstrate the inconsistency between thicknesses derived from boron concentration in solution and those determined by analysis of the polished side by TOF-SIMS and TEM/SEM measurements. In the reference experiment, there was a slight increase in values determined by solution concentration determination, but values for all methods were within a 15% uncertainty of the average.³⁰ With the addition of magnetite in the present work, a much larger discrepancy was observed between the methods as shown in Fig. 11.

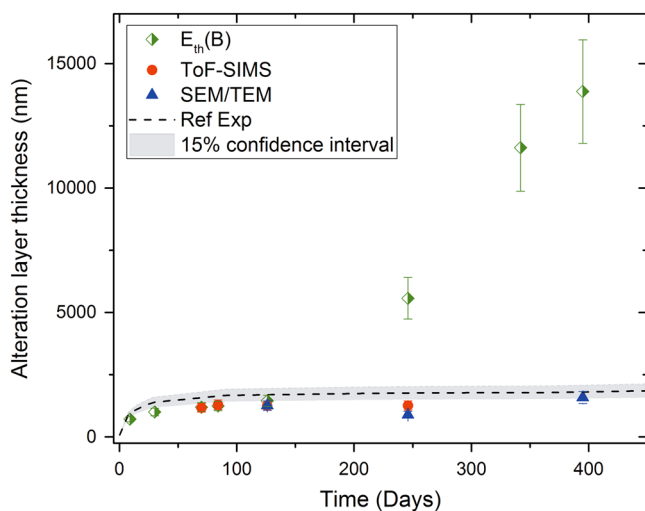


Fig. 11 Comparison of alteration layer thickness measurements. Agreement within all techniques is seen until alteration resumption. Physical measurements of the polished side of the monolith remain in agreement with the reference experiment.³⁰ Changes determined by increased concentrations of boron in solution highlight the effect of the alteration at surface cracks on the non-polished sides. Dotted line represents the alteration layer thicknesses determined in the reference experiment along with the corresponding 15% confidence interval

The three methods show agreement up until the alteration resumption. Even after this time there is not a significant change in the alteration layer thickness of the polished side that was analyzed by TOF-SIMS and SEM/TEM; the alteration layer thicknesses remain within error of the reference experiment even after the resumption of alteration. In similar experiments, a correction factor was included to account for the different rate of alteration of the rough non-polished surfaces.^{30, 31} It appears that the rough or cut surfaces show preferential alteration over the polished side. These reference experiments showed that the non-polished surfaces contributed to a surface area larger by a factor of 1.7, compared to calculations based on geometric considerations only. This correction is applicable to the first regime in the absence of magnetite. But even factoring in this difference, it does not explain the difference factor of 15 for the thicknesses (up to a localized factor of 70) obtained between solid and solution analysis. Moreover, a slight decrease of silicon concentration was observed between day 126 and day 246 data, but since the alteration layer should already be depleted in boron the correction factor does not explain this difference. It was found that the non-polished side had areas of large alteration that were centered on cracks in the surface that could begin to explain the discrepancies in thickness measurements.

Mechanisms of iron interaction

Many of the mechanisms detailed by Rebiscoul et al. were derived in this work, although it is difficult to distinguish between Si sorption and SiO_2 precipitation onto magnetite particles by methods used in this experiment.³⁵ It has to be assumed that both of these mechanisms (sorption and precipitation) were observed since the consumption of Si from solution was higher than can be accounted for by sorption only. The sorption capacity for magnetite has been measured to be $19 \pm 14 \mu\text{mol}$ of Si per gram of magnetite.⁵⁰ In this experiment, this sorption capacity only accounts for 7–80 p.p.m. of Si (allowing for the large error within the measurement provided by Philippini et al.) of the 120 p.p.m. loss observed over the first 2 months after the addition of

magnetite.⁵⁰ Since the mechanisms of sorption and SiO_2 precipitation cannot be separated, it can be speculated that sorption takes place within the first day after magnetite was added to the system. A decrease of 60 p.p.m. silica concentration from day 70 to day 71 falls within the range of 7–80 p.p.m. that can be accounted for by the sorption capacity. Thus, both sorption and SiO_2 precipitation mechanisms that occur at the magnetite surface seem to be predominant in the initial stages of the experiment, with the formation of secondary phases or a layer of iron at the glass surface only seen at later stage of the experiment.

In an additional experiment, International Simple Glass (ISG) grains of $\sim 5 \mu\text{m}$ diameter were altered in the same conditions as those tested here (pH 7, 90 °C, solution at equilibrium with amorphous silica) until 100% of boron had been released (complete alteration of the glass grains). The resulting grains can be considered as 100% alteration layer. The solubility of these altered grains were then measured, and after 100 days the system reached an equilibrium with a concentration of 43 p.p.m. of Si at pH 7. Data demonstrates that the alteration of the glass surface resumed when the concentration of Si in this experiment reached levels below this threshold of ~ 40 p.p.m. Si. This is also evident from the isotopic concentrations of Si in solution. After this threshold value of Si was reached, the glass, containing primarily ^{28}Si , begins to alter to re-establish the equilibrium in solution; this can be observed with the increase of ^{28}Si over ^{29}Si at day 246.

Monitoring the diffusion of methylene blue and lithium also gave insights on whether the incorporation of exogenous elements, such as iron, changed the properties of the alteration layer. It is possible that the introduction of iron into the alteration layer could reduce the porosity of the alteration layer and thus affect the ability of ions to diffuse. The GRAAL model predicts that the durability of glass waste forms are tied to the thermodynamic stability of the transport properties of the passivating layer.¹⁴ While we know that iron is detrimental to the durability glass, a layer that would restrict iron diffusion would be considered protective over time. As shown with Fig. 10, the iron rich layer did not limit the diffusion of small ions, Li in this case, into the pristine glass layer. Thus under these conditions, iron only decreases the stability of the system without providing any protective effect.

Effects of surface cracks

There is a large difference between the calculated alteration layer thicknesses by boron released and that experimentally observed on the monolith. This was due to the propagation of alteration within the cracks initially present on the rough surfaces of the glass monolith (see [Supplementary data](#)), a phenomenon that was unexpected when this study was designed. While the alteration layer on the polished side remained almost unaffected by the magnetite, the zones of alteration around the cracks extended up to $60\text{--}70 \mu\text{m}$ as shown in Fig. 8. The effects of these cracks must be carefully considered since actual waste packages are expected to have many cracks due to cooling of the glass and any possible stress fractures from movement of the canister.⁵¹ Though cracks within glass have been studied, few studies have been directly related to nuclear glasses under repository conditions.^{51, 52} These cracks substantially increase the surface area of the glass block along with providing areas with unique chemical environments. The localized conditions within these cracks provide a preferential site for quick alteration.

Stress fractures on the rough surfaces of the monoliths were also seen in the reference experiment, yet alteration in presence of magnetite progressed quicker than seen previously.³⁰ This could be due to the rapid change in solution conditions when magnetite was added to the system. Within the first 2 months after the addition of magnetite, the concentration of silicon decreased from a steady state of about 140 to around 20 p.p.m., with a decrease in 60 p.p.m. during the first day. This extreme change in solution

conditions caused the resumption of alteration and it was the surface cracks that provided sites for this alteration to reestablish the equilibrium between solution and the glass matrix.

Several studies have demonstrated that unique chemical environments exist within these cracks. The literature showed an increase in diffusion constants of ions, specifically Na, within the cracks when compared to the bulk glass.^{53, 54} The diffusion of these ions also creates a condensate region at the surface of the glass around the cracks. The pH in these regions increases compared to that of the bulk solution, which can lead to regions of increased silicate ion formation due to hydrolysis.⁵⁵ Therefore, crack formation is not specific to glasses in contact with iron, but iron can take advantage of these particular areas with unique chemistry in comparison with the bulk surface. This facilitates large regions of alteration that were not seen on the time scale of the reference experiment. Since the rate of propagation increases with an increasing crack length, the formation of these areas could be detrimental to the overall durability of the bulk glass.⁵⁶ Future studies will determine how the growing gel modifies the mechanical properties of the underlying glass, allowing new cracks to form.

METHODS

Experimental Set-up

ISG (SiO_2 56.2 wt%, B_2O_3 17.3 wt%, Na_2O 12.2 wt%, Al_2O_3 6.1 wt%, CaO 5.0 wt%, ZrO_2 3.3 wt%) was prepared by MoSci Corporation (Rollo, MO, USA). The glass was initially melted into ingots using platinum-rhodium crucibles at 1300 °C for about 4 h. The ingots were then annealed for 6 h at 569 °C before cooling to room temperature at a rate of 50 °C per hour. From one ingot, 8 monoliths of $2.00 \times 2.00 \times 0.11 \text{ cm}^3$ and eight monoliths of $0.50 \times 0.50 \times 0.11 \text{ cm}^3$ were obtained. One of the large faces of the monoliths were then polished to a mirror finish. The eight large monoliths were put into a Teflon holder and placed in the bottom of a 250 mL Teflon vessel in a vertical orientation. The smaller monoliths were wrapped in Teflon mesh and hung into solution from the top of the vessel as shown in Fig. 12.

The initial solution was saturated in amorphous $^{29}\text{SiO}_2$ (Eurisotop > 95% $^{29}\text{SiO}_2$) at $\text{pH}_{90^\circ\text{C}}$ 7. The isotopically tagged silica was melted with KOH (Suprapur) at 600 °C and the resulting soluble potassium silicate was then dissolved in 18 MΩ cm H_2O to obtain a concentration of 141 p.p.m. Si and 6900 p.p.m. K. Due to a small initial concentration of additional cations (i.e., sodium and calcium) an aliquot of the initial solution was characterized by ICP-OES for consideration of further calculations.

The total surface area was calculated as 76 cm^2 by geometric considerations. A previous study has found that the resulting reactive surface area due to only one polished face of the monolith is higher by a factor of 1.7, compared to the geometric surface area; the resulting reactive surface area was 129 cm^2 .³¹ The smaller monoliths contribute only a small fraction of the surface area and these monoliths are used for sampling throughout the experiment. The $\text{pH}_{90^\circ\text{C}}$ of the solution was maintained at 7.0 ± 0.5 using additions of 0.5 M KOH and 0.5 M HNO_3 , after 6 months pH was measured but not controlled.

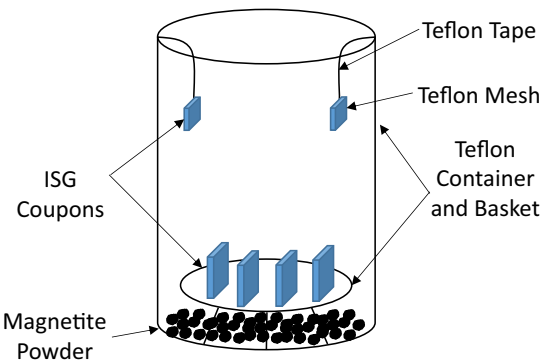


Fig. 12 Schematic of experimental set-up. Magnetite powder was added into the vessel at day 70

As the leaching solution was initially saturated with amorphous silica, the glass was altered in a residual rate until day 70, at which time the system was perturbed. Approximately 9.3 g of magnetite (Sigma Aldrich 0.48 μm average particle size) was added.

Solution analysis

Aliquots of solution were sampled regularly throughout the experiment for elemental concentration quantification by ICP-OES and silicon isotope ratios quantification by ICP-MS.⁵⁷ All samples and standards were purified using BioRad AG50 X-12 (200–400 mesh) cation exchange resin before silicon isotope analysis, as described in detail by Georg et al.⁵⁸ Silicon isotope ratio measurements were performed on a Thermo Scientific Neptune Plus Multi-Collector Inductively Coupled Plasma Mass-Spectrometer (MC-ICP-MS) at the Institut de Physique du Globe de Paris, France. All measurements were performed in static multicollection mode with Faraday cups attached to $10^{11} \Omega$ amplifier resistors. The Faraday amplifier gains were calibrated daily before the analytical session, yielding long-term reproducibility better than 10 p.p.m. The instrument was operated at medium resolution to avoid polyatomic interferences (e.g., $^{14}\text{N}^{16}\text{O}$, $^{14}\text{N}_2$, $^{12}\text{C}^{16}\text{O}$). The isotope beams of ^{28}Si , ^{29}Si , and ^{30}Si were measured using L3, C and H3 cups, respectively. A tandem cyclone-Scott type spray chamber Stable Introduction System (Thermo Scientific) with a PFA micro-flow nebulizer (ESI, USA) was used as the introduction system.

Boron solution concentrations were obtained by ICP-OES and were used to calculate the NL, the equivalent thickness (E_{th}) and subsequent rates (r) along with the altered glass fraction (AGF). The calculation for NL is shown in Eq. 4.

$$\text{NL}(\text{B}) = \frac{C_{\text{B}} \times V_{\text{solution}}}{((\text{SA}_{\text{small}} \times n_{\text{small}}) + (\text{SA}_{\text{large}} \times n_{\text{large}})) \times f_{\text{B}}} \quad (4)$$

where C_{B} is the concentration of boron in solution, V is the volume of solution, ρ is the density of glass which is 2.5 g cm^{-3} , SA is the calculated surface area of the glass, n is the number of monoliths remaining, and f_{B} is the fraction of boron in the glass (0.0537). The surface area and volume values were changed throughout the experiment as monoliths were sampled and corrected for any evaporation in the system. The equivalent thickness calculation is shown in Eq. 5 which is the NL divided by the glass density ρ_{glass} .

$$E_{\text{th}}(\text{B}) = \frac{\text{NL}(\text{B})}{\rho_{\text{glass}}} \quad (5)$$

The glass dissolution rate is calculated as shown with Eq. 6. This is determined by using a three point linear regression.

$$r = \frac{d(E_{\text{th}}(\text{B}))}{dt} \quad (6)$$

The AGF is determined by Eq. 7.

$$\text{AGF} = \frac{C_{\text{B}}}{f_{\text{B}} \times (V_{\text{glass}} \times \rho_{\text{glass}})} \quad (7)$$

where C_{B} is the concentration of boron in solution in g, f_{B} is the fraction of boron in the glass (0.0537), and V_{glass} is the addition of volume from each glass monolith in cm^3 .

The associated uncertainties for NL is 10%, E_{th} is 15%, while r is 30%.

The surface area is calculated based on the geometric surface area alone and does not take into account the physical surface area of the monolith. A factor of 1.7 is applied to the geometric surface area to correct for surface roughness of the unpolished surfaces for the calculation of surface area of each monolith, as previously explained.³¹ Additionally, the propagation of cracks on the unpolished surfaces of the monolith provided additional water accessible areas that impact the overall alteration of the glass monolith.

Solid analysis

Monoliths were sampled at multiple times throughout the experiment; day 70 (before addition of magnetite), day 83 (2 weeks after addition), day 126 (2 months after addition), day 246 (6 months after addition), and day 358 (9.5 months after addition). These monoliths were cut into four pieces for different analyses.

The polished face of the first four monoliths were analyzed by TOF-SIMS (IONTOF TOF 5) to visualize elemental profiles within the alteration layer. Two sputtering beams were used O_2^+ ($50 \times 50 \mu\text{m}^2$ area) or Cs^+ ($40 \times 40 \mu\text{m}^2$ area). The Cs^+ beam was used to analyze the H, and S ions while O_2^+

was used for all other ions. All ions are normalized to Zr, to minimize the matrix effects, as this element is immobile during alteration.⁵⁹

For monolith analysis by TEM, a thin section was extracted from the polished face of the sample and milled up to a thickness of ~100 nm. The sample was sputtered with an Au/Pd mixture and coated with Pt for protection. Observations and analyses were carried out with a Technai G2 (FEI) TEM microscope equipped with a LaB₆ source operating at 200 kV. A GATAN CCD camera, a BF-DF detector, and an EDX detector EDAX Genesis were used. The spatial resolution was 0.27 nm and the EDS spot size of 5 and 10 nm. For EDX analysis, the sample was tilted of 20° to minimize the overlaying of different phases. The counting time was 20 s to limit evaporation of mobile elements. SEM-EDS (JEOL JXA-8500 F) was also used to observe the alteration layers and surface features of the day-126 (polished face) and the day 358 (rough cut face) monoliths.

A post-experiment tracing was performed on the monoliths withdrawn at days 70, 83, 126, and 246. The monoliths were placed in a saturated amorphous ²⁸SiO₂ at pH 7 at room temperature for 100 h. The solution also contained 4.4 × 10⁻⁴ mol L⁻¹ methylene blue and 0.1 mol L⁻¹ LiCl. TOF-SIMS was performed on the polished face of the samples to study the diffusivity of these aqueous species into the developing alteration layers. This allowed for comparison to the reference sample to further understand the influence of iron on the properties of the alteration layer.

ACKNOWLEDGEMENTS

This research was performed using funding received from the U.S. DOE Office of Nuclear Energy's Nuclear Energy University Program under Project 23-3361 in addition to funding provided by the CEA, Areva, and the Chateaubriand Fellowship from the Embassy of France in the U.S. Authors warmly thank Laurent Dupuy at Biophy Research, France for the TOF-SIMS analysis, Martiane Cabié at Aix-Marseille University, France, for assistance with TEM, and CEA technical staffs for SEM analyses and Thibaut Martin for technical assistance.

AUTHOR CONTRIBUTIONS

L.N. initiated and was directly responsible for the experiment; she completed data analysis with the help of S.G. The article was also co-written by these two authors. A.G., T.D., and, T.E. performed MC-ICP-MS and TEM analysis. M.F. performed analysis of the unaltered monoliths. P.J. and N.W. acted as mentors for the experimental set up and editors throughout the writing process.

ADDITIONAL INFORMATION

Supplementary Information accompanies the paper on the *npj Materials Degradation* website (doi:10.1038/s41529-017-0001-6).

Competing interests: The authors declare that they have no competing financial interests.

Publisher's note: Springer nature remains neutral with regard to jurisdictional claims in published maps and institutional affiliations.

REFERENCES

- Donald, I. *Waste Immobilization in Glass and Ceramic Based Hosts: Radioactive, Toxic And Hazardous Wastes*. (Wiley, 2010).
- ANDRA (Agence Nationale pour la gestion des Déchets RAdioactifs). Dossier 2005: Andra research of the geological disposal of high-level long-lived radioactive waste. Results and Perspectives (2005).
- Gin, S. et al. An international initiative on long-term behavior of high-level nuclear waste glass. *Mater. Today* **16**, 243–248 (2013).
- Vienna, J. D., Ryan, J. V., Gin, S. & Inagaki, Y. Current understanding and remaining challenges in modeling long-term degradation of borosilicate nuclear waste glasses. *Int. J. Appl. Glass Sci* **4**, 283–294 (2013).
- Fleury, B. et al. Development of an experimental design to investigate the effects of r77 glass composition on the residual rate of alteration. *Procedia Mater. Sci* **7**, 193–201 (2014).
- Frugier, P., Martin, C., Ribet, I., Advocat, T. & Gin, S. The effect of composition on the leaching of three nuclear waste glasses: R77, AVM and VRZ. *J. Nucl. Mater.* **346**, 194–207 (2005).
- Gin, S., Beaudoux, X., Angéli, F., Jégou, C. & Godon, N. Effect of composition on the short-term and long-term dissolution rates of ten borosilicate glasses of increasing complexity from 3 to 30 oxides. *J. Non-Cryst. Solids* **358**, 2559–2570 (2012).
- Jantzen, C. M., Brown, K. G. & Pickett, J. B. Durable glass for thousands of years. *Int. J. Appl. Glass Sci* **1**, 38–62 (2010).
- Pierce, E. M. et al. Experimental determination of the effect of the ratio of B/Al on glass dissolution along the nepheline (NaAlSiO₄)-malinkoite (NaBSiO₄) join. *Geochim. Cosmochim. Acta* **74**, 2634–2654 (2010).
- Pierce, E. M., Rodriguez, E. A., Calligan, L. J., Shaw, W. J. & Pete McGrail, B. An experimental study of the dissolution rates of simulated aluminoborosilicate waste glasses as a function of pH and temperature under dilute conditions. *Appl. Geochem.* **23**, 2559–2573 (2008).
- Werne, L. O., Hench, L. L., Nogues, J.-L., Odelius, H. & Lodding, A. On the pH dependence of leaching of nuclear waste glasses. *J. Nucl. Mater.* **116**, 69–77 (1983).
- Andriambololona, Z., Godon, N. & Vernaz, E. R77 nuclear glass alteration in a saline medium: in situ experiments in the WIPP project. *Appl. Geochem.* **7**, 23–32 (1992).
- Jollivet, P. et al. Effect of clayey groundwater on the dissolution rate of the simulated nuclear waste glass SON68. *J. Nucl. Mater.* **420**, 508–518 (2012).
- Frugier, P. et al. SON68 nuclear glass dissolution kinetics: current state of knowledge and basis of the new GRAIL model. *J. Nucl. Mater.* **380**, 8–21 (2008).
- Grambow, B. & Muller, R. First-order dissolution rate law and the role of surface layers in glass performance assessment. *J. Nucl. Mater.* **298**, 112–124 (2001).
- McGrail, B. P., Ebert, W. L., Bakel, A. J. & Peeler, D. K. Measurement of kinetic rate law parameters on a Na-Ca-Al borosilicate glass for low-activity waste. *J. Nucl. Mater.* **249**, 175–189 (1997).
- Libourel, G. et al. The use of natural and archeological analogues for understanding the long-term behavior of nuclear glasses. *Comptes Rendus Geosci.* **343**, 237–245 (2011).
- Parruzot, B., Jollivet, P., Rébiscoul, D. & Gin, S. Long-term alteration of basaltic glass: mechanisms and rates. *Geochim. Cosmochim. Acta* **154**, 28–48 (2015).
- Verney-Carron, A., Gin, S., Frugier, P. & Libourel, G. Long-term modeling of alteration-transport coupling: application to a fractured Roman glass. *Geochim. Cosmochim. Acta* **74**, 2291–2315 (2010).
- Poinsot, C. & Gin, S. Long-term behavior science: the cornerstone approach for reliably assessing the long-term performance of nuclear waste. *J. Nucl. Mater.* **420**, 182–192 (2012).
- Doremus, R. H. Diffusion-controlled reaction of water with glass. *J. Non-Cryst. Solids* **55**, 143–147 (1983).
- Boksay, Z., Bouquet, G. & Dobos, S. Diffusion processes in surface layers of glass. *Phys. Chem. Glasses* **8**, 140–144 (1967).
- Ojovan, M. I., Pankov, A. & Lee, W. E. The ion exchange phase in corrosion of nuclear waste glasses. *J. Nucl. Mater.* **358**, 57–68 (2006).
- Gin, S. et al. The controversial role of inter-diffusion in glass alteration. *Chem. Geol.* **440**, 115–123 (2016).
- Doremus, R. H. Interdiffusion of hydrogen and alkali ions in a glass surface. *J. Non-Cryst. Solids* **19**, 137–144 (1975).
- Hench, L. Physical chemistry of glass surfaces. *J. Non Cryst. Solids* **25**, 343–369 (1977).
- Techer, I., Advocat, T., Lancelot, J. & Liotard, J. M. Dissolution kinetics of basaltic glasses: control by solution chemistry and protective effect of the alteration film. *Chem. Geol.* **176**, 235–263 (2001).
- Van Iseghem, P. et al. in *Environmental Issues and Waste Management Technologies in the Materials and Nuclear Industries XII* (eds Cozzi, A. & Ohji, T.) 115–126 (Wiley, 2009).
- Geisler, T. et al. Aqueous corrosion of borosilicate glass under acidic conditions: a new corrosion mechanism. *J. Non-Cryst. Solids* **356**, 1458–1465 (2010).
- Gin, S. et al. Origin and consequences of silicate glass passivation by surface layers. *Nat. Commun.* **6**, 6360 (2015).
- Gin, S. et al. The fate of silicon during glass corrosion under alkaline conditions: a mechanistic and kinetic study with the international simple glass. *Geochim. Cosmochim. Acta* **151**, 68–85 (2015).
- Valle, N. et al. Elemental and isotopic (Si-29 and O-18) tracing of glass alteration mechanisms. *Geochim. Cosmochim. Acta* **74**, 3412–3431 (2010).
- Fournier, M., Gin, S. & Frugier, P. Resumption of nuclear glass alteration: state of the art. *J. Nucl. Mater.* **448**, 348–363 (2014).
- Gin, S., Godon, N., Mestre, J. P., Vernaz, E. Y. & Beaufort, D. Experimental investigation of aqueous corrosion of R77 nuclear glass at 90°C in the presence of organic species. *Appl. Geochem.* **9**, 255–269 (1994).
- Rebiscoul, D. et al. Reactive transport processes occurring during nuclear glass alteration in presence of magnetite. *Appl. Geochem.* **58**, 26–37 (2015).
- Ribet, S. & Gin, S. Role of neoformed phases on the mechanisms controlling the resumption of SON68 glass alteration in alkaline media. *J. Nucl. Mater.* **324**, 152–164 (2004).

37. Bildstein, O., Trotignon, L., Perronet, M. & Jullien, M. Modelling iron-clay interactions in deep geological disposal conditions. *Phys. Chem. Earth Parts ABC* **31**, 618–625 (2006).

38. Burger, E. et al. Impact of iron on nuclear glass alteration in geological repository conditions: a multiscale approach. *Appl. Geochem.* **31**, 159–170 (2013).

39. Dillmann, P., Gin, S., Neff, D., Gentaz, L. & Rebiiscoul, D. Effect of natural and synthetic iron corrosion products on silicate glass alteration processes. *Geochim. Cosmochim. Acta* **172**, 287–305 (2016).

40. Godon, N., Gin, S. & Frugier, P. SON68 glass alteration enhanced by magnetite. *Procedia Earth Planet. Sci.* **7**, 300–303 (2013).

41. McVAY, G. L. & Buckwalter, C. Q. Effect of iron on waste-glass leaching. *J. Am. Ceram. Soc.* **66**, 170–174 (1983).

42. Michelin, A. et al. Archeological slag from Glinet: an example of silicate glass altered in an anoxic iron-rich environment. *Chem. Geol.* **413**, 28–43 (2015).

43. Michelin, A. et al. Silicate glass alteration enhanced by iron: origin and long-term implications. *Environ. Sci. Technol.* **47**, 750–756 (2013).

44. Kittel, C. *Introduction to Solid State Physics*. (Wiley, 2005).

45. Hed, P. & Edwards, D. Optical glass fabrication technology. 2: relationship between surface roughness and subsurface damage. *Appl. Opt.* **26**, 4677–4680 (1987).

46. Preston, F. W. The structure of abraded glass surfaces. *Trans. Opt. Soc.* **23**, 141–164 (1922).

47. Griffith, A. A. The phenomena of rupture and flow in solids. *Philos. Trans. R. Soc. Lond. Ser. Contain. Pap. Math. Phys. Character* **221**, 163–198 (1921).

48. Zapol, P., He, H., Kwon, K. D. & Criscenti, L. J. First-principles study of hydrolysis reaction barriers in a sodium borosilicate glass. *Int. J. Appl. Glass Sci.* **4**, 395–407 (2013).

49. Neeway, J. J. et al. Low-temperature lithium diffusion in simulated high-level boroaluminosilicate nuclear waste glasses. *J. Non-Cryst. Solids* **405**, 83–90 (2014).

50. Philippini, V., Naveau, A., Catalette, H. & Leclercq, S. Sorption of silicon on magnetite and other corrosion products of iron. *J. Nucl. Mater.* **348**, 60–69 (2006).

51. Mallet, C., Fortin, J., Guéguen, Y. & Bouyer, F. Evolution of the crack network in glass samples submitted to brittle creep conditions. *Int. J. Fract.* **190**, 111–124 (2014).

52. Ougier-Simonin, A., Guéguen, Y., Fortin, J., Schubnel, A. & Bouyer, F. Permeability and elastic properties of cracked glass under pressure. *J. Geophys. Res. Solid Earth* **116**, B07203 (2011).

53. Celarie, F., Ciccotti, M. & Marlière, C. Stress-enhanced ion diffusion at the vicinity of a crack tip as evidenced by atomic force microscopy in silicate glasses. *J. Non-Cryst. Solids* **353**, 51–68 (2007).

54. Wiederhorn, S. M., Guin, J.-P. & Fett, T. The use of atomic force microscopy to study crack tips in glass. *Metall. Mater. Trans. A* **42**, 267–278 (2010).

55. Wiederhorn, S. M., Fett, T., Guin, J.-P. & Ciccotti, M. Griffith cracks at the nanoscale. *Int. J. Appl. Glass Sci.* **4**, 76–86 (2013).

56. Freiman, S. W., Wiederhorn, S. M., Mecholsky, J. & John, J. Environmentally enhanced fracture of glass: a historical perspective. *J. Am. Ceram. Soc.* **92**, 1371–1382 (2009).

57. Alkiviadis, G. et al. Silicon isotope ratio measurements by inductively coupled plasma tandem mass spectrometry for alteration studies of nuclear waste glasses. *Anal. Chim. Acta* doi:10.1016/j.aca.2016.11.063.

58. Georg, R. B., Reynolds, B. C., Frank, M. & Halliday, A. N. New sample preparation techniques for the determination of Si isotopic compositions using MC-ICPMS. *Chem. Geol.* **235**, 95–104 (2006).

59. Cailleteau, C. et al. Insight into silicate-glass corrosion mechanisms. *Nat. Mater.* **7**, 978–983 (2008).



BY

Open Access This article is licensed under a Creative Commons Attribution 4.0 International License, which permits use, sharing, adaptation, distribution and reproduction in any medium or format, as long as you give appropriate credit to the original author(s) and the source, provide a link to the Creative Commons license, and indicate if changes were made. The images or other third party material in this article are included in the article's Creative Commons license, unless indicated otherwise in a credit line to the material. If material is not included in the article's Creative Commons license and your intended use is not permitted by statutory regulation or exceeds the permitted use, you will need to obtain permission directly from the copyright holder. To view a copy of this license, visit <http://creativecommons.org/licenses/by/4.0/>.

© The Author(s) 2017